OPEN ACCESS

ARTICLE

Journal homepage: www.the-innovation.org/energy-use

Energy Use

INNOVATION PRESS

Energy Use 2 (2025):100024

Contents lists available at INNOVATION PRESS

# High-speed Railway Thermal Management for Sustainable Future Transportation

**Tian You,[1,2,3,4,*] Yongzheng Zhang,[5] Zhaohui Sun,[5] Shuai Huang,[5] Dan Luo,[5] Jiankun Liu,[5,*] and Hongzhi Cui[1,2,3,4,*]**

*Correspondence: youtian@szu.edu.cn(T. Y.); liujiank@mail.sysu.edu.cn(J. L.); h.z.cui@szu.edu.cn(H. C.)

Received: ; Accepted: December 19, 2025; https://doi.org/10.59717/ipj.energy-use.2025.100024



## GRAPHICAL ABSTRACT

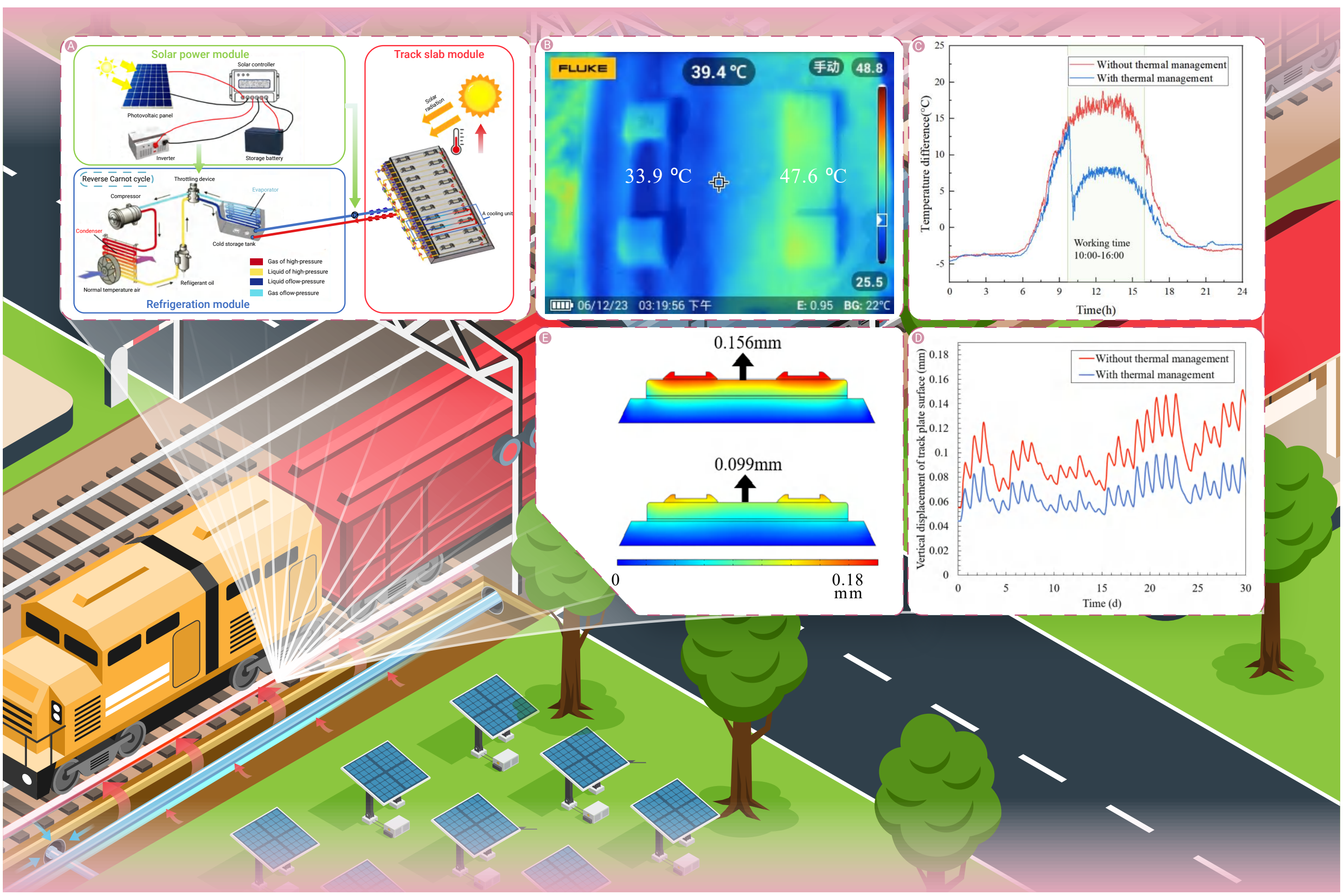


## PUBLIC SUMMARY

- Study proposes a thermal management system with cooling tubes for track slab temperature regulation.
- Multiphysics model reflects hydraulic-thermal-mechanical mechanisms in Guangzhou's hot climate.
- Cooling system reduces temperature difference by 70%, from 18.3°C to 6.7°C.
- Vertical displacement decreases by 40%, from 0.156 mm to 0.099 mm.
- Cooling tubes' heat transfer capacity reaches 2296 W, powered by renewable solar energy.

ARTICLE

Journal homepage: www.the-innovation.org/energy-use

Energy Use

INNOVATION PRESS

Energy Use 2 (2025):100024

Contents lists available at INNOVATION PRESS

# High-speed Railway Thermal Management for Sustainable Future Transportation

**Tian You,[1,2,3,4,*] Yongzheng Zhang,[5] Zhaohui Sun,[5] Shuai Huang,[5] Dan Luo,[5] Jiankun Liu,[5,*] and Hongzhi Cui[1,2,3,4,*]**

[1]College of Civil and Transportation Engineering, Shenzhen University, Shenzhen 518061, China
[2]Underground Polis Academy, Shenzhen University, Shenzhen 518061, China
[3]Key Laboratory of Coastal Urban Resilient Infrastructures (MOE), Shenzhen University, Shenzhen 518061, China
[4]Guangdong Engineering and Technology Research Center for Low-Carbon and Energy-Saving Buildings, Shenzhen University, Shenzhen 518061, China
[5]School of Civil Engineering, Sun Yat-Sen University, Zhuhai, Guangdong Province, 519082, China
*Correspondence: youtian@szu.edu.cn(T. Y.); liujiank@mail.sysu.edu.cn(J. L.); h.z.cui@szu.edu.cn(H. C.)
Received: ; Accepted: December 19, 2025; https://doi.org/10.59717/ipj.energy-use.2025.100024

Citation: You T., Zhang Y., Sun Z., et al. (2025). High-speed Railway Thermal Management for Sustainable Future Transportation. *Energy Use* 1:100024.

High-speed railways suffer from engineering damage, such as cracks and fractures, which are caused by the high internal temperature stress of the ballastless track slabs in hot climates. To address this issue, this study proposes a thermal management system using cooling tubes to actively regulate the temperature of the track slab. A multiphysics model of a high-speed railway in Guangzhou is established to reflect the hydraulic-thermal-mechanical mechanisms. Moreover, a full-scale experimental platform are established to monitor the dynamic temperature distribution of the track slab in hot climates in real-time and validate the numerical model. The study demonstrates that the maximum temperature difference of conventional ballastless track slabs can reach 18.3 °C, and the uniformity coefficient (UC) is 5.75. However, the thermal management system can effectively reduce the temperature difference by 70% to 6.7 °C, and the UC to 3.55. The corresponding vertical displacement decreases by 40% from 0.156 mm to 0.099 mm. The cooling tube's maximum heat transfer capacity is 2296 W, which is powered by renewable solar energy. Then, the factors that affect the system performance have been studied. This study can ensure the smooth and efficient operation of high-speed railways in hot climates.

## INTRODUCTION

Railways and high-speed railways play an important role in the economic development of many countries.[1,2] Specifically, in China, railways contribute significantly to the structural distribution of passenger transportation, accounting for 31.5% of the total in 2021.[3] Given the ambitious national high-speed railway development plan, which foresees the construction of numerous additional railway lines in the future, the demands for enhanced comfort and safety of high-speed railways are also expected to rise concomitantly. Currently, the primary track types employed in high-speed railways are categorized into two distinct groups: ballasted track slabs[4-6] and ballastless track slabs.[7-9] Given the ballastless track slab's advantages of high stability, superior flatness, and low maintenance requirements, it has progressively emerged as the primary structural configuration for high-speed railways.[10,11] Nevertheless, operational challenges arise when these slabs are deployed in hot climates. Specifically, under the influence of elevated ambient temperatures and intense solar radiation, the surface temperature of the ballastless track slab experiences a sharp increase, resulting in a significant temperature differential between its upper and lower surfaces. This temperature gradient subsequently generates high-temperature stress within the track slab, significantly altering its internal structural characteristics and mechanical properties. Manifestations of these changes include longitudinal forces and deformations along the track's longitudinal axis, as well as the development of cracks and fractures. Additionally, the temperature gradient along the depth direction can trigger temperature-induced warping deformation, leading to interlayer separation (commonly referred to as "seam") within the track slab.[12-15] These thermal-induced damages pose significant threats to the durability, ride comfort, and safety of high-speed railways. Given the global trend of climate warming,[16,17] the thermal damage phenomenon in ballastless track slabs is expected to become increasingly severe in the future. Therefore, it is imperative to devise effective measures to mitigate the temperature differential between the track slab surfaces and mitigate railway issues associated with hot climates.

A thermal management system is designed to regulate and control temperature or temperature gradients through heating or cooling mechanisms, tailored to the specific requirements of an object. Currently, its primary applications are in industrial domains, encompassing power batteries,[18,19] digital products, and the like. However, research on thermal management pertaining to track slabs remains scarce. Existing efforts have focused on passive temperature control methods.[20] For instance, phase change materials (PCM) have been incorporated into road construction. Jiang et al.[21] introduced a passive approach that employs PCM on the surface of track slabs, developing a novel thermal insulation reflective coating utilizing organic-inorganic PCM. This optimized PCM coating achieves a 36% reduction in the surface temperature of the track slab, thereby mitigating the concrete's temperature rise and the temperature gradient within the ballastless track slab under high-temperature conditions. To address the thermal arching and damage issues associated with Type II ballastless tracks in China, Zhang et al.[22] proposed a passive method involving a high reflective metal-ceramic anticorrosive coating. Experimental and simulation results indicate that the temperature gradient of the track slab with a 300 μm metal-ceramic anticorrosive coating decreased by 29%. Nevertheless, these passive solutions offer only limited relief from the high surface temperature of track slabs, lacking the ability to actively and effectively manage the temperature field.

Active thermal management of track slabs represents an efficacious approach to mitigating thermal damage in high-speed railways operating in hot climates. One such approach involves the embedding of tubes within road structures or concrete. Xiang et al.[23] introduced a photovoltaic thermal-ground source heat pump (PVT-GSHP) system tailored for solar roads, wherein tubes are integrated into the solar road and interconnected with a ground heat exchanger (GHE). This system effectively extracts heat from the road, thereby reducing the temperature of photovoltaic cells (PVCs) and storing the extracted heat in the soil to elevate soil temperatures. This approach significantly contributes to enhancing the efficiency of photovoltaic power generation and optimizing the operational performance of ground source heat pumps (GSHPs). Furthermore, researchers such as Zhou et al.[24] have explored the incorporation of cooling tubes in concrete to mitigate hydration heat, preventing the development of cracks in large concrete blocks during the construction phase. However, hydration heat originates internally and concentrates at the center of the concrete mass, whereas the heat in ballastless track slabs primarily results from solar radiation absorption, concentrated on the surface. Given the distinct nature of heat generation and location in these two applications, the cooling techniques employed differ significantly.

In our previous study,[25] we proposed an active temperature control method wherein cooling tubes are strategically positioned near the upper surface within the track slab. These tubes are connected to a refrigeration system, allowing low-temperature water to circulate and dissipate heat from the track slab, thus reducing the surface temperature. Our results indicate that this approach can reduce the surface temperature difference of the track slab by up to approximately 70% in hot regions, effectively regulating the temperature field within the track slab. However, our previous work did not encompass the design and integration of a refrigeration or power generation system. Additionally, the previous two-dimensional modeling approach limits our ability to comprehensively assess the performance of the active thermal management system. To address these limitations, we aim to develop a three-dimensional model that incorporates the refrigeration and power generation systems, enabling a more comprehensive evaluation of the system's performance and optimization of its design.

Hence, in this study, a comprehensive thermal management system encompassing both refrigeration and power generation subsystems is delineated. Additionally, a numerical hydraulic-thermal-mechanical coupling model is formulated for the track slab in Guangzhou, aimed at investigating the specific attributes of the temperature field, stress field, and pipeline flow field of the ballast-less track slab in a hot climate. Subsequently, an experimental platform for track slabs integrated with a thermal management system is constructed to validate the developed model. Following this, a detailed analysis is conducted to assess the temperature distribution, deformation characteristics, and operational performance of ballast-less track slabs under the influence of a thermal management system in a hot climate. Concurrently, the influential factors pertaining to thermal management are examined. This research endeavor aims to mitigate the deformation issues stemming from uneven temperature distribution in ballast-less track slabs, thereby ensuring the unhindered and efficient operation of high-speed railways in hot climates.

## THE BALLASTLESS TRACK SLAB WITH A NOVEL THERMAL MANAGEMENT SYSTEM

A thermal management system of the track slab using cooling tubes can solve engineering problems such as seams and fractures of high-speed railway structure layer caused by uneven temperature distribution in the ballastless track slab under high-temperature conditions.[25] This section will introduce the specific structure, detailed principle, and operation scheme of the thermal management system.

### Principle of the thermal management system

High-speed railway lines are predominantly located in open fields, and instances of thermal damage to these lines are frequently caused by the combined effects of intense solar exposure and high-temperature weather conditions. To address this issue, the proposed temperature regulation system capitalizes on the abundant solar energy resources available along lines at risk of thermal damage. It harnesses solar power to drive a compression refrigeration module, employing water or refrigerant as the circulating medium to cool the ballastless track slab. By utilizing a clean and renewable energy source, this system only necessitates the initial investment for the solar power generation equipment and incurs minimal maintenance costs. Furthermore, it operates without ongoing energy expenses and produces no carbon emissions, thus contributing positively to environmental protection. The proposed thermal management system comprises three modules: a track slab module, a refrigeration module, and a solar power module, as illustrated in Figure 1A.

The refrigeration module is the cold source of the thermal management system, as shown in Figure 1A. It produces low-temperature water for the track slab module through a refrigeration unit. The refrigeration unit consists of a compressor, a condenser, a throttling device and an evaporator. The refrigeration principle is the reversed Carnot cycle.[27,28] The evaporator is placed in the cold storage tank as the cold source, and the temperature controller regulates it to produce the cooling water at a certain temperature. Then the low-temperature water is pumped to the cooling tube inside the track slab module.

The solar power module is the power source of the thermal management system, as shown in Figure 1A. The power is generated by a photovoltaic panel using renewable solar energy. This module includes a solar controller, a photovoltaic panel, a storage battery, and an inverter. Solar energy is directly converted into electricity by the semiconductor interface of the photovoltaic panel.[29] The inverter converts the direct current generated by the photovoltaic panel into alternating current for the use of refrigeration module and other devices.

The operational strategy of the thermal management system for high-speed railways is elaborated in detail for hot climatic conditions. When solar radiation is intense, the solar power generation module exhibits high efficiency and generates substantial electricity, converting solar energy into electrical energy to drive the refrigeration module or store it in batteries. When the temperature sensor detects a high surface temperature of the track slab, the refrigeration module automatically activates, pumping low-temperature water into the cooling tube. The cooling water extracts heat from the track slab surface, thereby reducing the surface temperature of the track slab and minimizing the temperature differential. Once the temperature sensor senses that the track slab has reached an appropriate surface temperature, the thermal management system automatically ceases operation.

During overcast conditions with low solar radiation intensity, the efficiency of the solar power generation module diminishes, resulting in insufficient power generation. In such cases, the stored energy in the batteries can be combined to drive the refrigeration module. In fact, under low solar radiation intensity, the surface temperature of the track slab is relatively lower, necessitating a smaller cooling capacity. During nighttime when there is no solar radiation, the photovoltaic panels are unable to generate electricity, and the track slab does not experience thermal damage issues, thus eliminating the need for temperature regulation.

### Configuration and heat transfer of the track slab with cooling tubes

The track slab module diagram is shown in Figure 1. It consists of multiple cooling tubes buried near the upper surface of the track slab, which can actively control its temperature distribution. The tubes are made of copper because of their high thermal conductivity (401 $W \cdot m^{-1} \cdot K^{-1}$) among metals. The cooling tubes are arranged under the stirrup with a protective layer thickness of 3~4 cm to reduce the impact of trains running on the railway.

Previous papers[25] show that the polyline-buried cooling tube, which follows the upper surface of the track slab, has a better cooling effect than the straight-buried cooling tube. Therefore, as Figure 1C shows, the polyline-buried cooling tube is used at the cross-section with sleepers in this paper. Besides, the straight-buried cooling tube is used at the cross-section without sleepers shown in Figure 1B. A cooling unit consists of two polyline-buried cooling tubes, one straight-buried cooling tube, and one returning tube. As Figure 1A shows, a standard CRTS II track slab is 6.45 m long and can be buried with five cooling units in parallel through branch joints.

As shown in Figure 1D, the thermal management system aims to actively regulate the internal temperature of the track slab by using convective and conductive heat transfer. Water flows inside the cooling tube to facilitate heat transfer because of its high specific heat capacity (4200 $J \cdot kg^{-1} \cdot K^{-1}$) and stable cooling effect. In summer, low-temperature water flows in the cooling tube and effectively removes the heat from the upper surface of the track slab through the following processes: non-isothermal water convection, water-tube wall convection (Equation 1), tube wall conduction, and tube wall-concrete conduction (Equation 2).[26] This way, the track slab can withstand

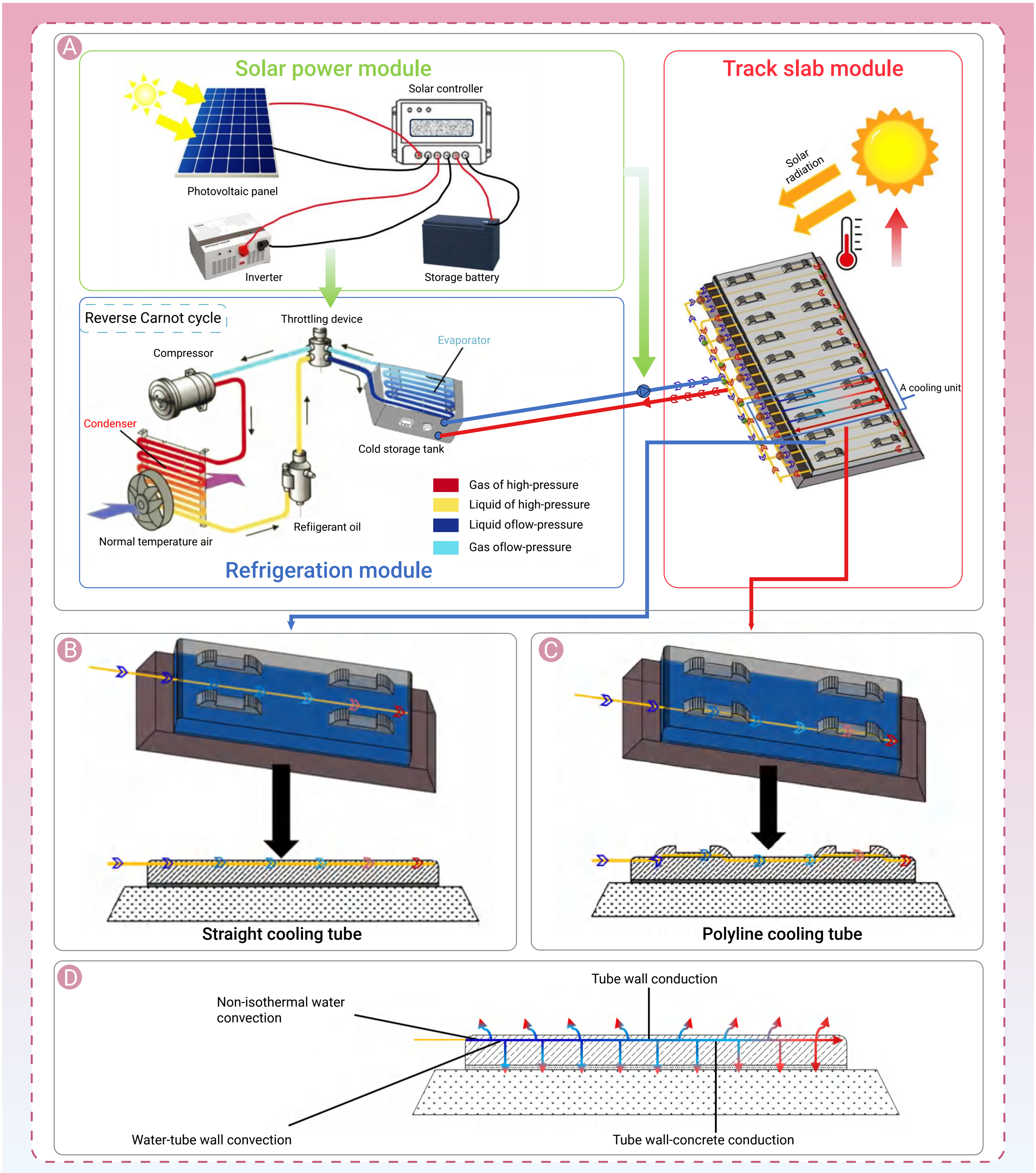


**Figure 1. Schematic diagram and principle of track slab module of the thermal management system** (A) Overall diagram; (B) Diagram of a straight cooling tube; (C) Diagram of a polyline cooling tube; (D) Heat transfer inside the track slab。

high ambient temperature and strong solar radiation, and its surface temperature can be lowered actively.

$$\frac{\partial t}{\partial \tau}+u\frac{\partial t}{\partial x}+v\frac{\partial t}{\partial y}+w\frac{\partial t}{\partial z}=\frac{\lambda}{\rho C_p}\left(\frac{\partial^2 t}{\partial x^2}+\frac{\partial^2 t}{\partial y^2}+\frac{\partial^2 t}{\partial z^2}\right) \tag{1}$$

In the Equation 1, the first term on the left is an unsteady term, which indicates the temperature change rate over time. The second, third and fourth terms are convection terms and represent heat transfer due to fluid motion. The right-hand side of the equation is the diffusion term and represents heat transfer due to fluid conduction.

$$\frac{\partial}{\partial x}\left(k\frac{\partial T}{\partial x}\right)+\frac{\partial}{\partial y}\left(k\frac{\partial T}{\partial y}\right)+\frac{\partial}{\partial z}\left(k\frac{\partial T}{\partial z}\right)+q=\rho C_p\frac{\partial T}{\partial t} \quad (2)$$

where $t$ is time; x, y and z are coordinate axes; $\rho$ is the material density, $kg/m^3$; $C_p$ is the specific heat capacity of the material, $J/(kg\cdot K)$; $k$ is the thermal conductivity of the material, $W/(m\cdot K)$.

## MATERIALS AND METHODS

To investigate the temperature field of track slabs, several methodologies are commonly employed, including analytical solutions, numerical simulations, and experimental tests. When juxtaposed against analytical solutions, numerical simulations exhibit an advantage in comprehensively and precisely computing the three-dimensional temperature distribution within the track slab, fluid dynamics within the cooling tubes, and soil temperature patterns. Furthermore, when compared to experimental testing, numerical simulations facilitate easier modifications of design specifications and boundary conditions, thereby enabling an analysis of the impact of various factors. Consequently, this study utilizes the finite element method, implemented via COMSOL software, to construct a numerical model of the CRTS II plate-type ballastless track slab and investigate its thermal management performances.

To ascertain the veracity of the simulation results, an experimental setup featuring a track slab equipped with a thermal management system has been devised. This platform serves to evaluate system performance and validate the simulation findings. The present section delves into the simulation methodology, parameter configuration, and model validation through the experiment. Additionally, it introduces indexes for assessing temperature uniformity and energy consumption.

### Three-dimensional coupled hydraulic-thermal-mechanical model

***Physical and geometric model.*** This paper employs COMSOL Multiphysics software to simulate the interplay between the temperature field, stress field, and non-isothermal pipeline flow within the ballastless track slab of a Guangzhou high-speed railway. The ballastless track and subgrade model adhere to the specifications of the standard CRTS II type prefabricated track slab, which measures 6.45 meters in length and supports 20 sleepers, as illustrated in Figure 2A. The precise dimensions align with the cross-section depicted in Figure 2C for the standard CRTS II ballastless track slab.

Constructed from reinforced concrete, the track slab has a width of 2.55 meters and a thickness of 0.2 meters. The cement-emulsified asphalt (CA) mortar layer is 2.55 meters wide and 0.03 meters thick. Beneath this, a plain concrete bearing layer spans 3.25 meters in width and 0.3 meters in thickness. To minimize discrepancies between the computational domain and actual semi-infinite soil conditions, the simulated ground domain extends to 7 meters in width and 20 meters in depth. The subgrade comprises viscous loess positioned below the bearing layer. Table 1 details the calculated parameters for the track slab, CA mortar layer, bearing layer, and subgrade.

***Parameters and boundary conditions.*** The solid heat transfer module in Comsol software is used to simulate the three-dimensional heat transfer in the track slab, and the transient heat transfer is governed by Equation (3).

$$\rho_s C_{p,s}\frac{\partial T_s}{\partial t}+\rho_s C_{p,s} v\cdot\nabla T_s+\nabla\cdot q=Q+Q_{ted} \quad (3)$$

$$q=-k_s\nabla T_s \quad (4)$$

where $T_s$ is the solid temperature at each physical layer, °C; $\rho_s$ is the density of the solid at each physical layer, $kg/m^3$; $C_{p,s}$ is the specific heat capacity of the solid, $J/(kg\cdot K)$; $v$ is the velocity vector, $m/s$; $Q$ is the heat source, $W$; $k_s$ is the thermal conductivity of the solid, $W/(m\cdot K)$.

The boundary conditions of the three-dimensional geometric model are set as follows: both sides of the foundation (AH and FG sections in Figure 2C) are adiabatic boundaries.[30] The bottom of the foundation (HG section in Figure 2c) is a constant soil temperature of 20.0 °C.[31] The surfaces of the foundation (sections AB and EF in Figure 2c) have a given ground surface temperature. The upper surface of the track slab (sections BCDE in Figure 2c) absorbs solar radiation with the radiation absorption rate of 0.6.[32] The upper surface of the track slab also has a convective heat transfer with the air, as shown in Equation (6). According to experimental results in the literature,[33] the convective heat transfer coefficient on the concrete surface can be calculated from the wind speed. In addition, the track slab will also emit heat radiation, and its radiation heat transfer can be determined according to Stefan-Boltzmann's formula,[34,35] and the effective radiation heat flux of the track slab surface in the air is calculated according to Equation (8). The ambient temperature, ground surface temperature, solar radiation intensity, and wind speed required for boundary conditions are all derived from hourly data from meteorological databases[36] in typical years.

$$q_{sr}=aQ_s \quad (5)$$

where $q_{sr}$ is the heat flux radiated by the sun to the surface of a track slab, $W/m^2$; $a$ is the absorption rate of solar radiation on the surface of the track slab; $Q_s$ is the solar radiation intensity, $W/m^2$.

$$q_{ch}=-\lambda\frac{\partial T_s}{\partial n}=h(T_a-T_s) \quad (6)$$

$$h=3.06u_w+4.11 \quad (7)$$

where $q_{ch}$ is the heat flux of convective heat transfer between track slab and environment, $W/m^2$; $T_a$ is the air temperature at the boundary, °C; $h$ is the heat transfer coefficient of the track slab surface, $W/(m^2\cdot K)$; $u_w$ is the wind speed, $m/s$.

$$q_{rh}=\varepsilon\sigma\left[(T_{sky}+273.15)^4-(T_s+273.15)^4\right] \quad (8)$$

$$\varepsilon=\frac{1}{\frac{1}{\varepsilon_c}+\frac{1}{\varepsilon_a}-1} \quad (9)$$

$$T_{sky}=T_a-14 \quad (10)$$

where $q_{rh}$ is the heat flux of radiative heat transfer between the track slab and the environment, $W/m^2$; $T_{sky}$ is the sky effective temperature, °C; $\sigma$ is Stefan Pohl's Hertz constant, $5.67\times10^{-8}W/(m^2\cdot K^4)$; $\varepsilon$ is the net blackness coefficient, calculated according to Equation (9), where the concrete blackness coefficient can be $\varepsilon_c=0.88$, the atmospheric blackness coefficient is $\varepsilon_a=0.88$.

To study the deformation of the track slab simultaneously, the solid mechanic's module in Comsol software is adopted, and its governing equation is as shown in Equation (11).

$$\rho_s\frac{\partial^2 u_2}{\partial t^2}=\nabla\cdot\sigma+F_v \quad (11)$$

where $\rho_s$ is the density at each physical layer, $kg/m^3$; $u_2$ is displacement field; $\sigma$ is stress, $N/m^2$; $F_v$ is bulk load, $N$.

To couple solid heat transfer and solid mechanics, a multi-physical field coupling module of thermal expansion should be added. The governing equation for this module is shown in Equation (12).

$$\varepsilon_{th}=\alpha(T)(T_s-T_{ref}) \quad (12)$$

where $\varepsilon_{th}$ is a linear strain caused by temperature changes; $\alpha(T)$ is the linear expansion coefficient of the material, $1/K$; $T_s$ is the temperature of the physical model, °C; $T_{ref}$ is the initial reference temperature of the physical model, °C.

To simplify the calculation, only the structural layers above the subgrade (track slab, CA mortar layer, and bearing layer) are set in the calculation domain of the solid mechanical physical field. Specifically, the bottom boundary BE is set as a fixed constraint; the side boundary is supported by the roller shaft, and the other boundary is free.

The non-isothermal pipe flow module in Comsol software is used to simulate the heat transfer of the cooling tube in the thermal management system, and its governing equations are as follows: Equations (13) to (15).

$$\frac{\partial A\rho_f}{\partial t}+\nabla g(A\rho_f u_f)=0 \quad (13)$$

$$\rho_f\frac{\partial u_f}{\partial t}=-\nabla p_f-\frac{1}{2}f_D\frac{\rho_f}{d_h}|u_f|u_f \quad (14)$$

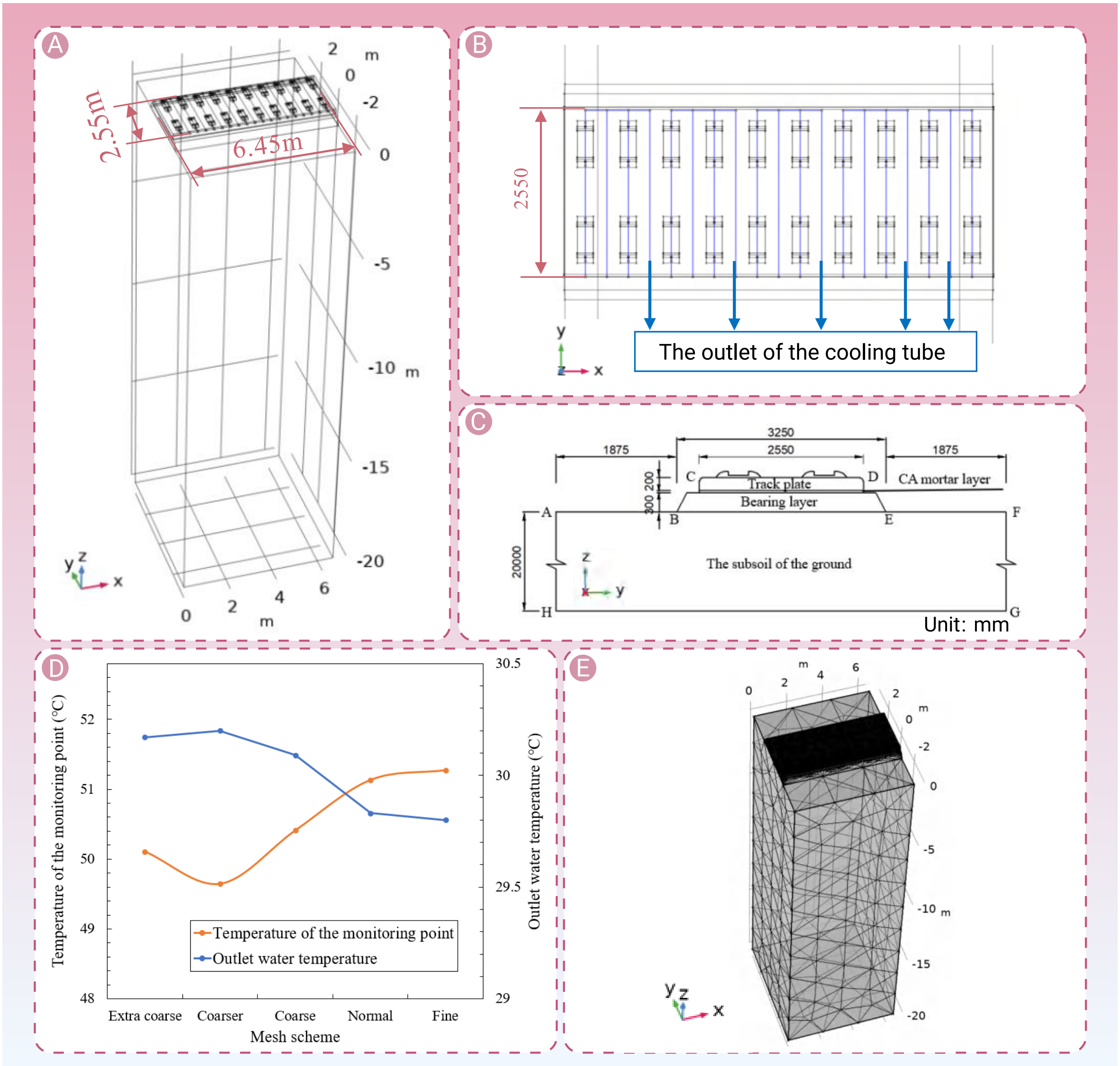


**Figure 2. Numerical model of a ballastless track slab with the thermal management system** (A) Three-dimensional geometric model of the track slab; (B) Diagram of cooling tube arrangement; (C) The cross-section of the geometric model of the track slab; (D) Outlet water temperature and monitoring point temperature under different mesh schemes; (E) The final grid distribution.

Table 1. Properties of each structure layer

| Structure layer | Density ($kg·m^{-3}$) | Thermal conductivity ($W·m^{-1}·K^{-1}$) | Specific heat capacity ($J·kg^{-1}·K^{-1}$) | Coefficient of linear expansion ($1·K^{-1}$) | Young's modulus (Pa) |
| --- | --- | --- | --- | --- | --- |
| Track slab | 2551 | 2.33 | 920 | $10 \times 10^{-6}$ | $35.5 \times 10^{9}$ |
| CA mortar layer | 1800 | 1.43 | 1050 | $10 \times 10^{-6}$ | $24 \times 10^{9}$ |
| Bearing layer | 2300 | 1.80 | 970 | $10 \times 10^{-6}$ | $32 \times 10^{9}$ |
| Subgrade | 1650 | 1.78 | 1500 | / | / |

$$\rho_f A C_{p,f}\frac{\partial T_f}{\partial t} + \rho_f A C_{p,f} u_f g \nabla T_f = \nabla g A k_f \nabla T_f + \frac{1}{2} f_D \frac{\rho_f A}{d_h}|u_f|^3 + Q_{wall} \tag{15}$$

where $\rho_f$ is the fluid density, $kg/m^3$; $u_f$ is the average cross-sectional velocity of fluid, $m/s$; $p_f$ is the fluid pressure, $N/m^2$; $C_{p,f}$ is the specific heat capacity of the fluid, $J/(kg \cdot K)$; $T_f$ is the temperature of the fluid, $°C$; $k_f$ is the thermal conductivity of the fluid, $W/(m \cdot K)$; $d_h$ is the hydraulic diameter, m;

Table 2. Grid sensitivity analysis

| Mesh scheme | Grid number | Outlet water temperature | Temperature of the monitoring point | Time consumption |
|---|---|---|---|---|
| Extra coarse | 39964 | 30.17°C | 50.11°C | 1min 4s |
| Coarser | 49154 | 30.20°C | 49.65°C | 1min 5s |
| Coarse | 58740 | 30.09°C | 50.41°C | 1min 7s |
| Normal | 139113 | 29.83°C | 51.13°C | 3min 35s |
| Fine | 808782 | 29.80°C | 51.27°C | 32min 5s |

$\frac{1}{2}f_D\frac{\rho_f}{d_h}|u_f|u_f$ represents the pressure drop due to viscous shear; $Q_{wall}$ is the heat source term of the tube wall.

The cooling tube is a copper pipe with an inner diameter of 6 mm and a wall thickness of 1 mm. As shown in Figure 2B, a cooling unit consists of four parallel cooling tubes, and multiple cooling units are connected in parallel. The cooling tube passing through the sleeper is polyline, and that passing through the sleeper is straight, as shown in Figure 1. The boundary conditions are set as follows: the inlet flow rate of the cooling tube is 0.6 m/s, and the inlet temperature is 25 °C. The outlet boundary is heat outflow and a standard atmospheric pressure of 101325 Pa. The wall of the cooling tube is set as a wall layer to simulate the conductive heat transfer.

In this paper, the initial non-uniform soil temperature is calculated by the 30-year' heat transfer simulation between the air and the land. Then, the dynamic temperature field of the high-speed railway track slab and subgrade is simulated hourly by applying the above boundary conditions. Starting from August 1, the coupling simulation of the three physical fields of hydraulic, thermal, and mechanical is carried out for the newly built track slab with a thermal management system. The simulation takes one hour as a step, the simulation time is the whole month of August, and the relative tolerance is set as 0.0001.

***Grid sensitivity analysis.*** To determine the appropriate mesh, the calculation accuracy of models with different mesh qualities is investigated for the steady-state calculation.[37] The corresponding grid number, the outlet water temperature of the cooling tube, the monitoring point temperature in the track slab, and the calculation time are shown in Table 2 and Figure 2D.

Through grid sensitivity analysis, it can be found that the normal grid can achieve similar calculation results as the fine ones, and its grid number is significantly reduced compared to the fine ones. So, the normal grid not only reduces the calculation time, but also makes the calculation results more accurate. Therefore, an extremely fine grid is used near the cooling tube, and a normal grid is used for the rest calculation domain. The whole model has 139,113 grids, as shown in Figure 2E.

### *Full-scale experiment of the* ballastless track slab

To ensure the accuracy of simulation results, we established a test platform of CRTS II plate-type ballastless track in Zhuhai, where has similar climate to Guangzhou. Real-time observation of track slab temperature changes was conducted, and the experimental findings were subsequently utilized to validate our model.

***Experimental setup.*** A segment of a standard CRTS II slab, incorporating two longitudinal sleepers, was constructed as depicted in Figure 3. The structure was layered successively from the bottom up, consisting of the subgrade bearing layer, CA mortar, and track slab. Six copper tubes, each with a 6 mm inner diameter, were embedded 3 cm beneath the surface of the track slab to serve as cooling tubes. Additionally, a connector for the main tube was specially designed to interface with the refrigeration module. The temperature monitoring setup included the TOPRIE1000 temperature acquisition instrument, which was interfaced with 48 T-type thermocouples positioned in the upper, middle, and lower sections of the track slab. This configuration allowed for temperature measurements with an accuracy of ±0.5 °C.

The refrigeration module comprises a 120 W compressor, an air-cooled condenser, a capillary tube serving as a throttling device, and a copper tube evaporator. These components are assembled as illustrated in Figure 1B. The refrigeration system is charged with R134a refrigerant to facilitate the cooling cycle. Meanwhile, the solar power module includes a 200 W single-crystal solar photovoltaic panel, a 200ah storage battery, a solar controller, an inverter, and a supporting photovoltaic bracket. The connection of these elements follows the schematic shown in Figure 1A. The integrated setup of the refrigeration module and solar module is presented in Figure 3A.

***Testing result and validation.*** Firstly, the temperature distribution of the track slab without a thermal management system was monitored under hot climatic conditions. Under intense solar radiation, the surface temperature of the track slab experienced a significant increase, peaking at 53.2 °C at 1:00 pm. In contrast, the bottom temperature reached its maximum of 37.7 °C five hours later, specifically at 6:00 pm. This observation indicates a five-hour delay between the peaks of the upper and lower temperatures. Further analysis revealed that the maximum temperature difference between the upper and lower surfaces of the track slab occurred at 2:00 pm, reaching a value of 18.7 °C.

Then, the temperature distribution of the track slab equipped with a thermal management system was closely monitored through field full-scale experiments conducted in a hot climate. The operational period of the thermal management system was designated from 10:00 to 16:00, during which the refrigeration temperature of the compressor was maintained at 15 °C. A comparative analysis was conducted by positioning one sleeper under the control of the thermal management system, while the other sleeper remained without such a system. As depicted in the infrared camera image (Figure 4B), the temperatures recorded near the sleeper with thermal management and without thermal management were 33.9 °C and 47.6 °C, respectively. This comparison provides insights into the effectiveness of the thermal management system in regulating the temperature of the track slab. According to Figure 4A, based on the experimental data, the temperature differential between the upper and lower surfaces of the track slab, in the absence of thermal management, ranges from 9.7 °C to 18.7 °C. Conversely, when equipped with a thermal management system, the temperature difference is significantly reduced, ranging from 1.0 °C to 7.0 °C. This demonstrates the efficacy of the thermal management system in minimizing both the surface temperature and the temperature gradient within the track slab.

Concurrently, the experimental setup was utilized for model validation. A numerical model of the experimental platform was constructed, and the recorded meteorological data was utilized as input to simulate the temperature field of the track slab without a thermal management system. Figure 4C presents a comparative analysis of the track slab surface temperature obtained from both experimental and simulation methods. The experimentally measured upper surface temperature of the track slab ranged between 29.1 °C and 53.2 °C, while the corresponding simulated values spanned from 29.8 °C to 53.5 °C. Similarly, the experimentally recorded lower surface temperature varied from 31.5 °C to 37.7 °C, while the simulated range was 32.2 °C to 38.8 °C. Both experimental and simulation results exhibited comparable trends. Figure 4D further compares the temperature nephograms of the track slab at 1:00 pm, revealing a substantial consistency between the results of both methods. These experimental findings validate the accuracy and reliability of the adopted simulation methodology.

### Evaluation indexes

To evaluate the temperature controlling effect of the thermal management system, several evaluation indexes are defined. Temperature gradient (gradT) and uniformity coefficient (UC) evaluate the temperature uniformity within the track slab. The heat transfer rate and the total heat transfer indicate the energy consumption of the thermal management system.

The temperature gradient in the track slab is the ratio of the temperature difference to the distance between two points in the track slab, which can be

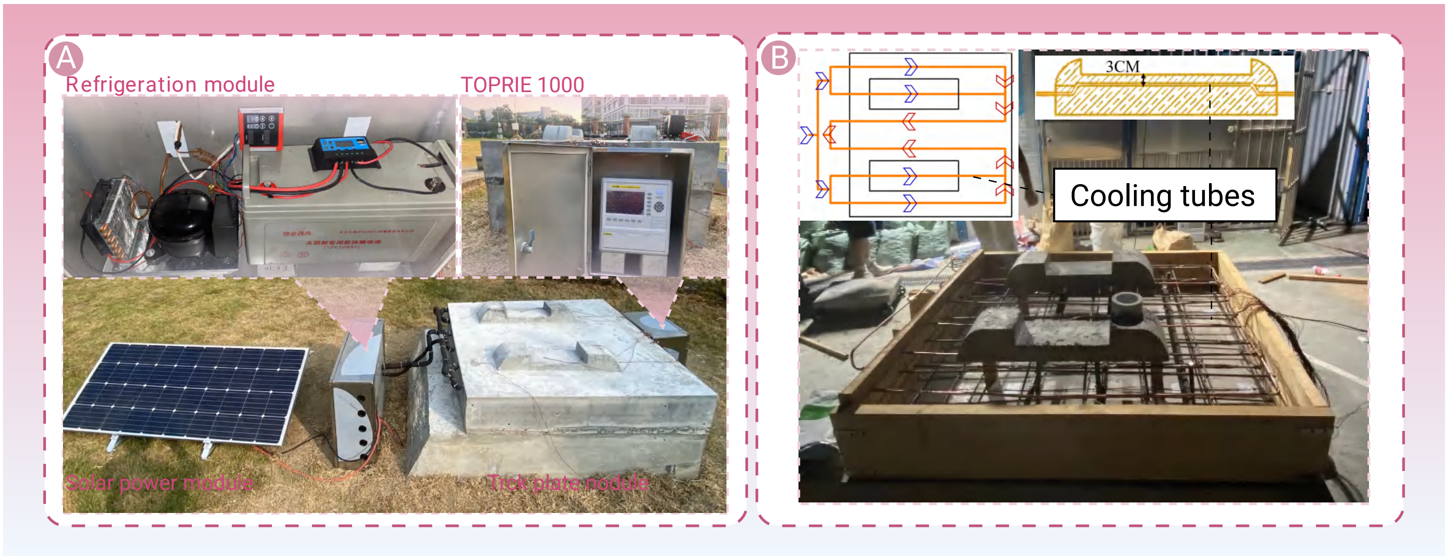


**Figure 3. Experimental setup** (A) Thermal management system overview; (B) Cooling tube arrangement

calculated by Equation (16).

$$\mathrm{grad}T = \frac{\Delta T}{\Delta d} \tag{16}$$

where ΔT is the temperature difference between two points in the track slab, *ºC*; Δd is the distance between two points in the track slab, *m*.

UC is the standard deviation of temperatures of typical points in the track slab, which can be calculated by Equation (17).

$$UC = \sqrt{\frac{1}{n}\left[(T_1-\overline{T})^2+(T_2-\overline{T})^2+\cdots(T_n-\overline{T})^2\right]} \tag{17}$$

where n is the number of sampling points in the track slab; $T_{1,2,3\ldots n}$ are the temperatures of each sampling point, *ºC*; $\overline{T}$ is the average temperature in the track slab domain, *ºC*.

A large gradT and a large UC indicate a low uniformity of temperature distribution in the track slab, and vice versa.

The heat transfer rate is the heat transfer capacity of the cooling tube per meter in length, which is calculated by Equation (18).

$$q = \frac{Q}{L} \tag{18}$$

where *Q* is the total heat transfer of the cooling tube, *W*; *L* is the length of the cooling tube, *m*.

The total heat transfer is the sum of the heat transfer of all the cooling tubes in the thermal management system, which is calculated by Equation (19). It is mathematically equivalent to the integral of the heat transfer rate in the length. In COMSOL, we can obtain the value from line integrals.

$$Q = \sum Q_{t1} + Q_{t2} + Q_{t3} + Q_{t4} + \cdots\cdots Q_{tn} \tag{19}$$

where $Q_{t1}$, $Q_{t2}$, $Q_{t3}$, $Q_{t4}$, $\cdots\cdots Q_{tn}$ is heat transfer capacity of each cooling tube, *W*.

## RESULTS AND ANALYSES

To fully reflect the control effect of the thermal management system on the temperature and deformation of the track slab, a coupled hydraulic-thermal-mechanical ballastless track slab model with thermal management system has been established. The three-dimensional temperature field and stress field of the track slab, and internal hydraulic-thermal coupling field inside the tube buried in the track slab will be simulated and analyzed. The three-dimensional temperature field can reflect the temperature control effect of the thermal management system on the track slab. The three-dimensional stress field will reflect the stress distribution of the track slab, and show the improvement of temperature control on the mechanical performance of the track slab. The hydraulic-thermal coupling field inside the cooling tube buried in the track slab reflects the cooling performance and energy consumption characteristics of the thermal management system. Therefore, this section will comprehensively analyze the temperature regulation and deformation control effect of the ballastless track slab with thermal management under hot weather.

### Three-dimensional temperature field of the track slab

The three-dimensional temperature field of the track slab without and with thermal management system is shown in Figure 5A & B. The thermal management system effectively reduces the overall temperature of the track slab.

The temperature distribution of the track slab and its dynamic temperature variation over time in August are analyzed in this section. Figure 5C shows the temperature changes of the upper and lower surfaces of the track slab with and without the thermal management system. The thermal management system significantly reduces the upper surface temperature of the track slab but has little effect on the lower surface. Specifically, the upper and lower surface temperatures of the track slab without thermal management varies greatly, and the temperature of the upper surface (25.5 ~54.7 °C) is much higher than that of the lower surface (28.4 ~41.1 °C). With the thermal management system, the temperature of the upper surface (25.1 ~39.0 °C) is much smaller than before, and the temperature range of the lower surface is 27.0 ~35.8 °C. This is because the cooling tube is placed closer to the upper surface of the track slab, which has a stronger cooling effect on the upper surface to reduce the surface temperature. Figure 5D shows the corresponding temperature difference between the top and lower surfaces of the track slab. Thermal management greatly reduces the surface temperature difference of the track slab. In particular, the surface temperature difference of the track slabs without thermal management ranges in -6.4 °C ~ 18.3 °C, and that with thermal management ranges in -5.4 °C and 6.7 °C.

Y-Z cross-section temperature nephograms of the track slab with and without the thermal management system at 2:00 pm on August 20, as shown in Figure 5E & F. The central temperature at the upper surface of the track slab without the thermal management system is as high as 54.7 °C, and the central temperature at the lower surface is about 36.4 °C. The temperature difference between them is 18.3 °C, and the temperature gradient along the depth direction is 0.915 °C/cm. At noon, due to the higher ambient temperature and stronger solar radiation, the upper surface temperature of the track slab is higher than the lower surface temperature, and the temperature difference reaches the daily maximum.[38-41] In contrast, the central temperatures of the upper and lower surface of the track slab with thermal management system are controlled at 39.0 °C and 32.3 °C respectively. The temperature difference between them decreases by nearly 65% to 6.7 °C, and the temperature gradient along the depth decreases to 0.335 °C/cm. Therefore, thermal management technology by adding cooling tubes can significantly reduce the temperature gradient along the depth and

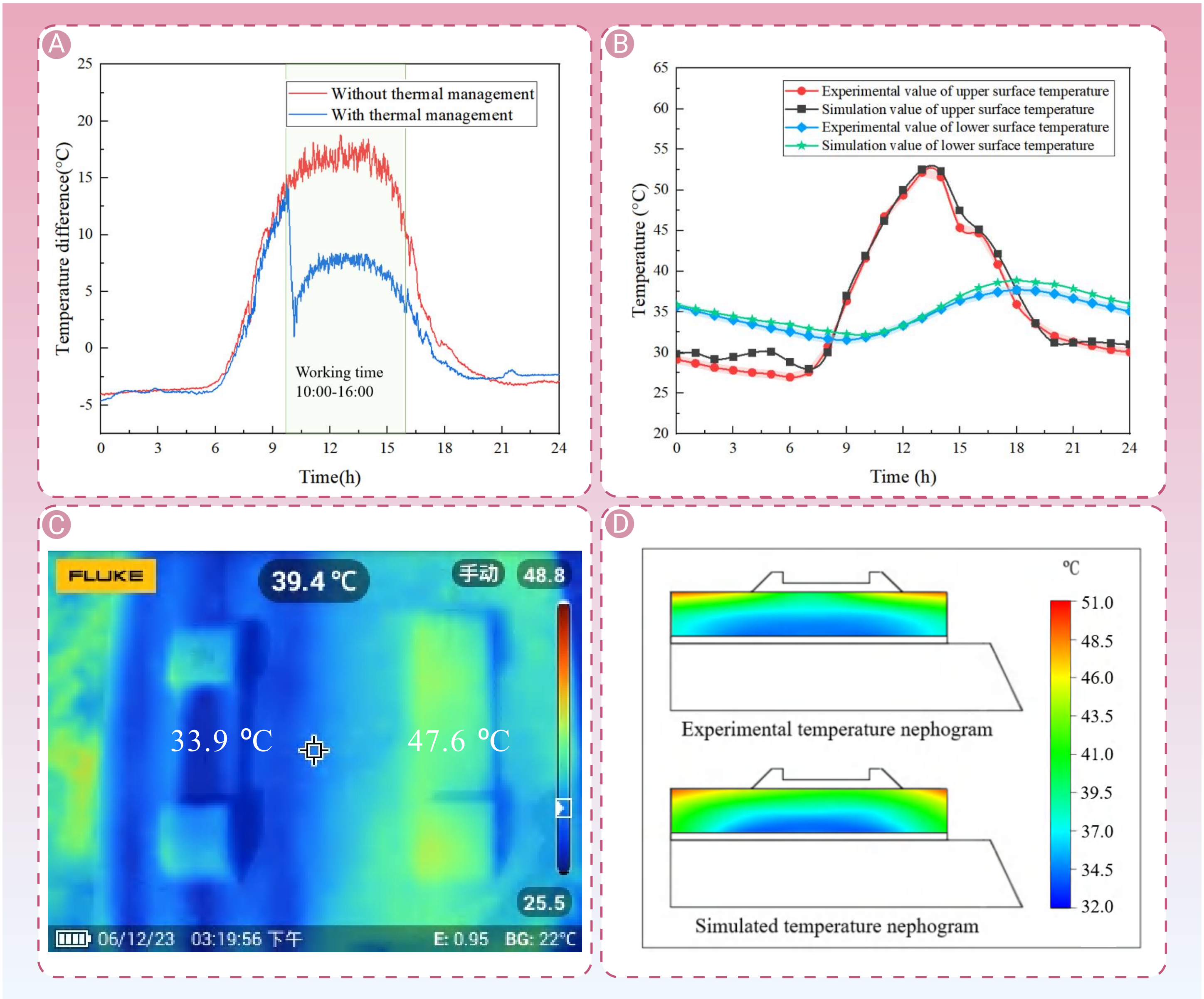


**Figure 4. Testing result and validation** (A) Temperature differences between upper and lower surfaces of track slab; (B)Thermal imaging on the surface of the track slab; (C) Comparison of dynamic track slab surface temperature between experiment and simulation; (D) Comparison of track slab temperature nephogram at 13:00 between experiment and simulation

temperature difference between the upper and lower surfaces of the track slab.

Figure 5G & H shows the comparison of X-Z cross-section temperature nephograms of the track slab with and without the thermal management system. Along the length, the temperature is lower near the cooling tube. This has two effects: first, the surface temperature of the track slab with thermal management is lower than that of the track slab without thermal management. Second, the temperature gradient in the depth direction of the track slab with thermal management is smaller than that without thermal management.

In the three-dimensional field of the track slab, points are selected every 4 cm in the x, y and z axis, and a total of 50,800 points are uniformly selected to calculate the UC of the track slab by equation (17). The thermal management system can reduce the temperature unevenness of the track slab. Specifically, the average temperatures in the track slab with and without thermal management are 36.3 °C and 43.9 °C respectively. The corresponding UC of the track slab with and without thermal management is 3.55 and 5.75 respectively.

Without thermal management, a ballastless track slab has a large temperature difference between its upper and lower surfaces in a hot climate, leading to a large temperature gradient along its depth. This makes the temperature distribution of the track slab uneven. The thermal management system can lower the surface temperature of the track slab effectively, and thus reduce both the surface temperature difference and the temperature gradient along its depth. This makes the temperature distribution of the track slab more uniform along its depth.

## Three-dimensional displacement field of the track slab

Thermal damages in ballastless track slabs are attributed to excessive temperature gradients and displacement along the depth direction. This section delves into the displacement characteristics of the track slab along the depth direction (the z-axis). Figure 6A & B presents a comparative analysis of the three-dimensional deformation of the track slab along the z-axis, both without and with the implementation of a thermal management system. Notably, the incorporation of the thermal management system significantly reduces the overall vertical displacement of the track slab.

Figure 6C depicts the deformation in the depth direction on the upper surface of the track slab, comparing scenarios with and without thermal management during the month of August. In the absence of thermal management, the deformation in the depth direction is substantial, spanning

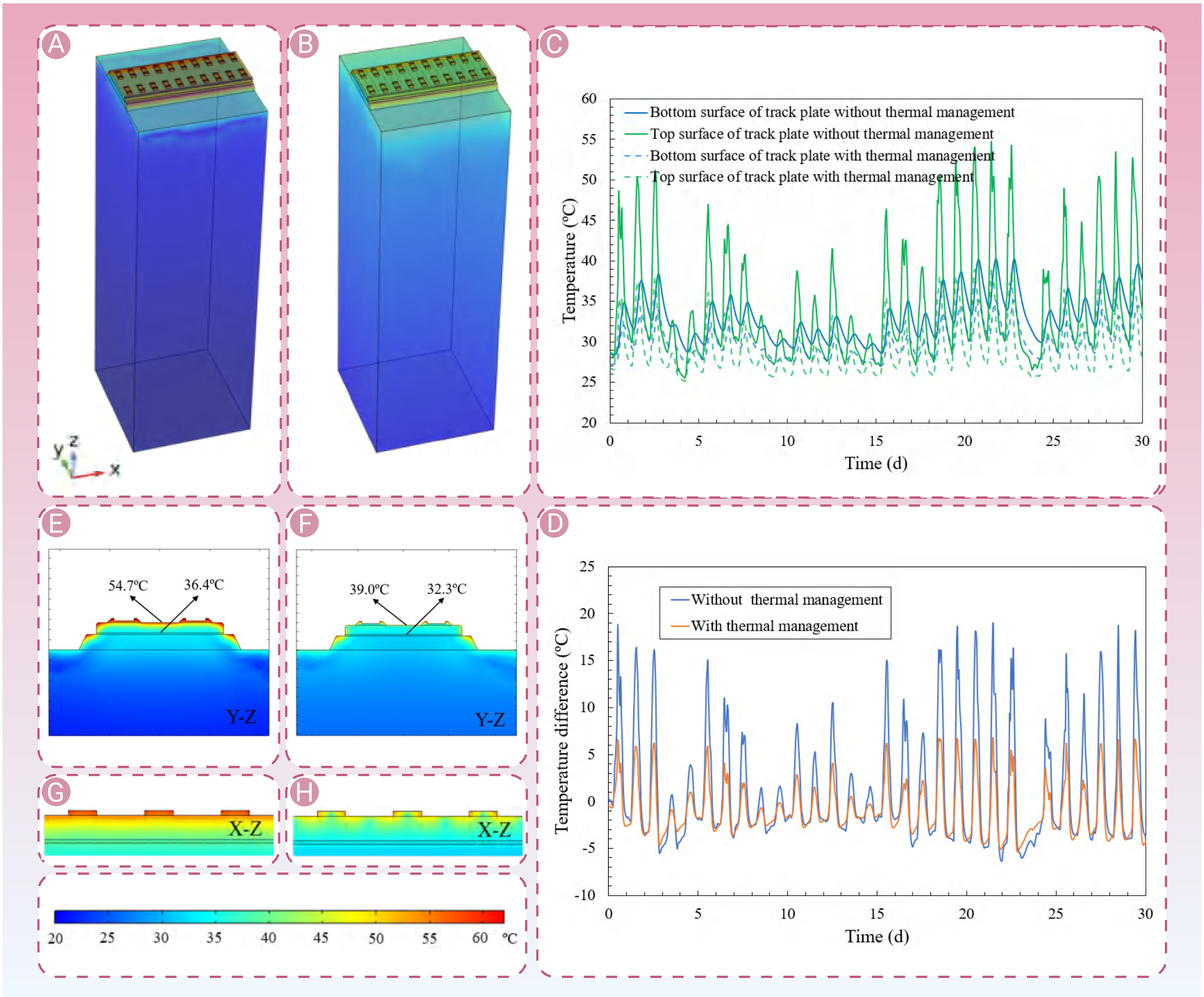


**Figure 5. Three-dimensional temperature field** (A) Three-dimensional temperature field without thermal management; (B) Three-dimensional temperature field with thermal management; (C) Dynamic temperature of top and lower surfaces of track slabs; (D) Comparison of temperature difference between top and lower surfaces of track slab; (E)&(F) Y-Z cross-section temperature nephogram of track slab without and with thermal management; (G)&(H) X-Z temperature nephogram of part track slab without and with thermal management.

a range from 0.068 mm to 0.156 mm. Conversely, with the implementation of thermal management, this deformation is notably diminished, ranging from 0.044 mm to 0.099 mm. A comparative analysis reveals that the depth-wise deformation of the track slab with thermal management is reduced by approximately 40% compared to its counterpart without thermal management. This significant reduction underscores the effectiveness of thermal management in minimizing track slab deformation along the depth direction, thereby mitigating the potential for warping.

In this study, the track slab without a thermal management system attains its peak vertical displacement at 17:00 on August 30. Figure 6D presents a comparative analysis of the Y-Z cross-sectional contour nephogram, depicting the depth-wise deformation of the track slab both with and without a thermal management system at this specific time. As evident from Figure 6D, the absence of a thermal management system results in an upward deformation of 0.156 mm at the central upper surface of the track slab, indicating the influence of temperature stress. Conversely, the introduction of a thermal management system mitigates this deformation, reducing it to 0.099 mm. This observation underscores the efficacy of thermal management systems in mitigating temperature-induced deformations in track slabs. In hot climates, the track slab has a large displacement along the depth direction due to the temperature stress caused by the high temperature gradient of the track slab. The thermal management system can effectively lower this displacement and solve the deformation problem of the ballastless track slab railway in hot summer.

## Temperature fields inside the cooling tubes

In this section, the temperature field within the cooling tubes is investigated, and the thermal performance of the thermal management system is assessed by considering the inlet and outlet water temperatures, the heat transfer rate, as well as the total heat transfer.

Figure 7A illustrates the inlet and outlet water temperatures of the cooling tube recorded during a one-month simulation. The inlet water temperature is maintained at a constant 25 °C to facilitate heat dissipation from the track slab. Consequently, the outlet water temperature elevates to a range of 25.1 °C to 27.4 °C, representing an average increase of approximately 0.7 °C compared to the inlet temperature. Specifically, at the 494-hour mark, as depicted in Figure 7B, the outlet water temperature attains its maximum value of 27.4 °C.

Figure 7C presents the daily total heat transfer of the cooling tube during the operation of the thermal management system. Under conditions where

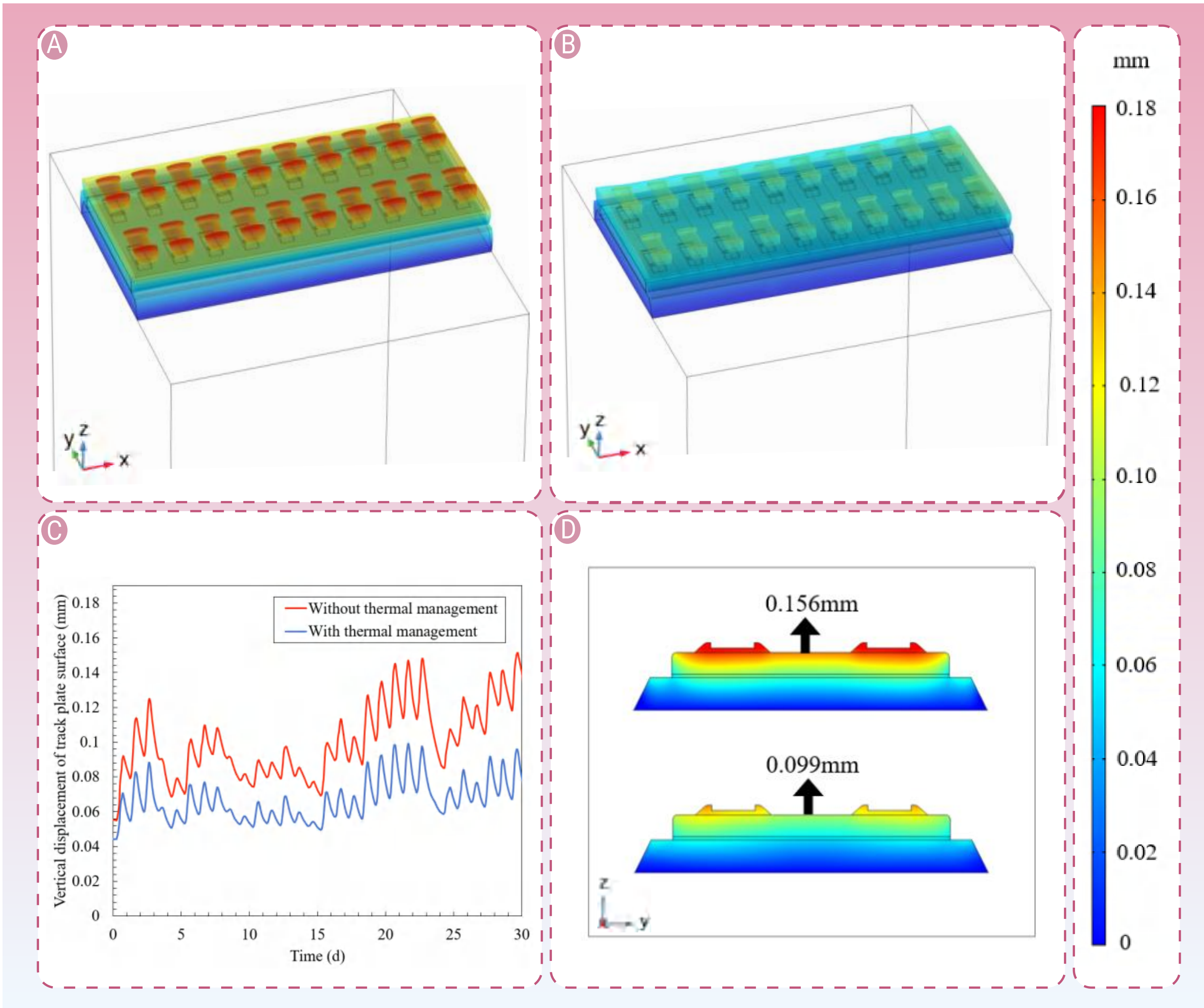


**Figure 6. Three-dimensional displacement field** (A) Vertical displacement of a three-dimensional track slab without thermal management system; (B) Vertical displacement of a three-dimensional track slab with thermal management system; (C) Dynamic vertical displacement comparison of track slab surface; (D) Comparison of vertical displacement nephogram of the cross section of the track slab

the circulating flow rate and inlet temperature in the cooling tube are maintained at 0.6 m/s and 25 °C respectively, the average total heat transfer is observed to be 750 W, with a maximum value of 2296 W. Notably, on August 20, the heat transfer rate of the cooling tube peaks. Accordingly, Figure 7D illustrates the hourly dynamic heat transfer rate and total heat transfer of the cooling tube specifically on that day. When solar radiation is intense, the thermal management system assumes an important role in controlling the temperature of the track slab. Specifically, at 14:00 on that day, both the heat transfer rate and total heat transfer of the cooling tube attains their respective maxima of 41.72 W/m and 2296 W.

## DISCUSSION

In Result Section, a comprehensive analysis has been conducted to examine the impact of the thermal management system on a high-speed railway track slab, encompassing temperature control, stress mitigation, heat transfer inside the cooling tube. Notably, the operation condition and tube design within this system also significantly influence the thermal regulation of the track slab. Therefore, the thermal management system should be optimized from the aspects of operation conditions and the tube designs. To address this, the section compares the effects of temperature gradients, vertical deformations, and heat exchange on the track slabs by adjusting various parameters such as cooling temperatures, fluid velocities, tube diameters, and cooling tube interconnections. This approach aims to achieve an optimal design and ultimately enhance the overall thermal management efficacy.

### The optimization of operating conditions

The operating parameters encompass the cooling temperature and the flow velocity. Based on the model of track slab integrated thermal management outlined in section 3.1, the optimal cooling temperature is studied. The optimization is conducted by systematically adjusting the inlet temperature of the cooling tube in increments of 5 °C, ranging from 15 °C to 30 °C, while maintaining a constant state for all other boundary conditions.

Figure 8A shows how the inlet temperature of the cooling tube affects the surface temperature difference, vertical displacement, UC, and total heat transfer of the track slab. As expected, the lower the inlet temperature of the cooling tube, the greater the heat transfer temperature difference with the track slab, which leads to a smaller temperature difference on the track slab surface, a smaller vertical displacement, but a larger total heat transfer. When the inlet water temperature rises from 15 °C to 30 °C, the surface temperature difference increases from 4.4 °C to 8.1 °C; the vertical displacement

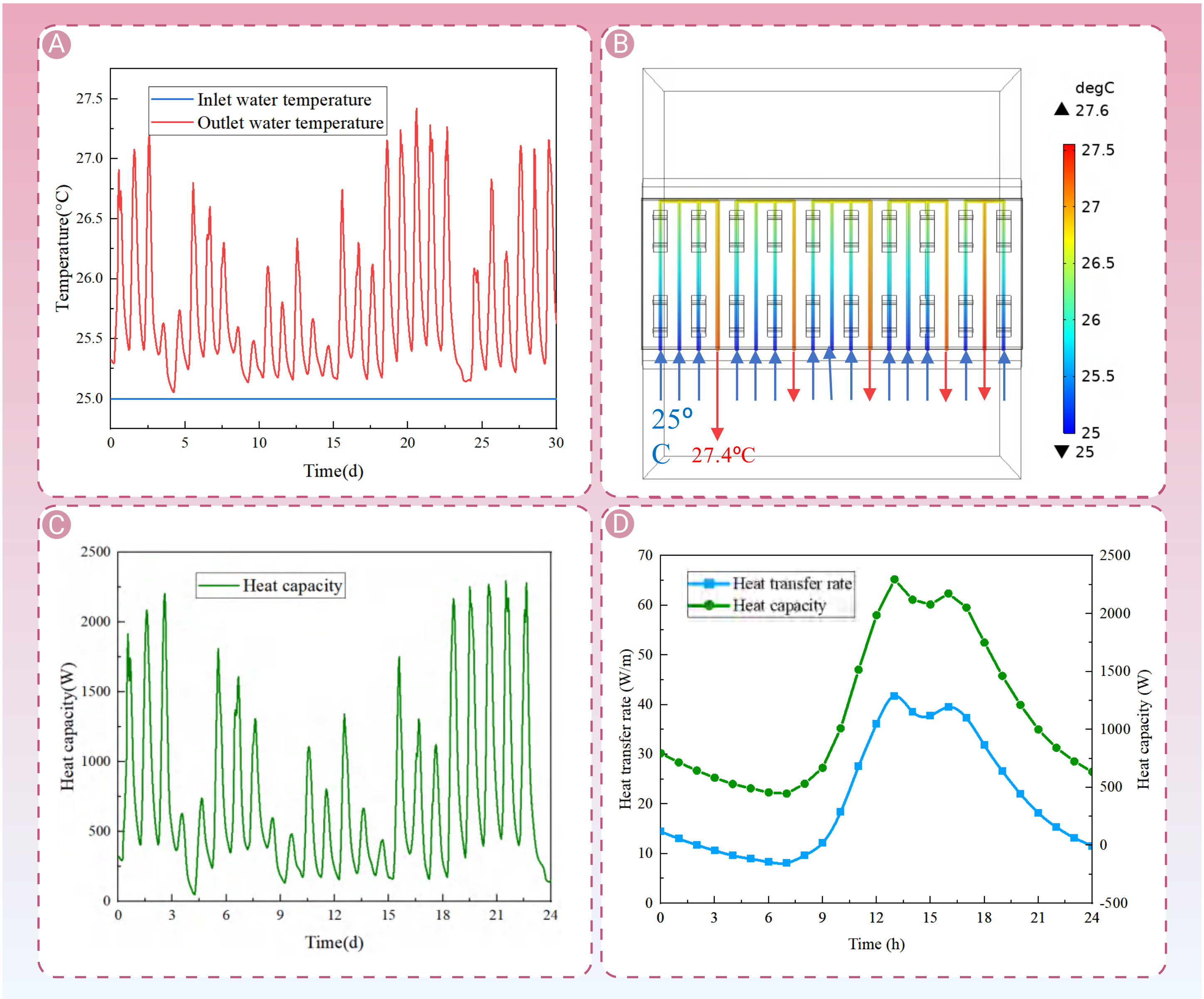


**Figure 7. Temperature fields of non-isothermal pipe flow** (A) Dynamic inlet and outlet water temperature of the cooling tube; (B) Temperature field of the cooling tube at 14:00 on August 20; (C) Dynamic heat transfer rate and total heat transfer of cooling tube; (D) The heat transfer rate and total heat transfer of the cooling tube on August 20

increases from 0.072 mm to 0.111 mm; and the total heat transfer decreases from 1904 W to 3057 W. The uniformity of the temperature inside the track slab first improves and then deteriorates as we increase the inlet water temperature. The optimal inlet water temperature should be 25 °C which gives us a minimum UC value of 3.55 for the track slab. This means that the cooling temperatures should not be too high or too low because they will either fail to cool down the surface of the track slab or create an uneven temperature distribution inside it.

Figure 8B shows the effect of different flow velocities on the surface temperature difference, vertical displacement, UC, and total heat transfer of the track slab. To find the optimal flow velocity, the flow velocity of the cooling tube is increased from 0.2 m/s to 0.8 m/s with a step size of 0.2 m/s while keeping other boundary conditions unchanged. As expected, a higher flow velocity of the cooling tube means a higher convective heat transfer coefficient inside the tube, which leads to a smaller surface temperature difference and a smaller vertical displacement of the track slab but a larger total heat transfer. When the flow velocity changes from 0.2 m/s to 0.8 m/s, the surface temperature difference decreases from 7.4 °C to 6.6 °C; the vertical displacement decreases from 0.100 mm to 0.098 mm; and the total heat transfer increases from 2058 W to 2328 W. The uniformity of the temperature inside the track slab improves as we increase the flow velocity until it reaches a minimum UC value of 3.55 for both 0.6 m/s and 0.8 m/s circulation velocities. However, compared with the heat transfer (2328 W) at the flow velocity of 0.8 m/s, the heat transfer (2296 W) at the flow velocity of 0.6 m/s is smaller. To maintain track slab uniformity and promote energy conservation, the optimal flow velocity is determined to be 0.6 m/s.

In summary, it is investigated the influence of different operating conditions of the cooling tube on the performance of the thermal management system. This was achieved by varying the inlet water temperature and flow velocity. Among these two operating parameters, the inlet water temperature demonstrates the most significant impact on the system's performance. The results indicate that an optimal inlet water temperature of 25°C yields the best thermal management effect. Additionally, it was found that an optimal flow velocity of 0.6 m/s contributes to effective thermal management. These findings provide valuable insights for optimizing the operation of thermal management systems.

### The optimization of cooling tube designs

In addition to the operating conditions discussed in previous section, the design of the cooling tube, specifically its diameter and connection configuration, also significantly impacts the performance of the thermal management system. To ascertain the optimal design for the cooling tube, a three-

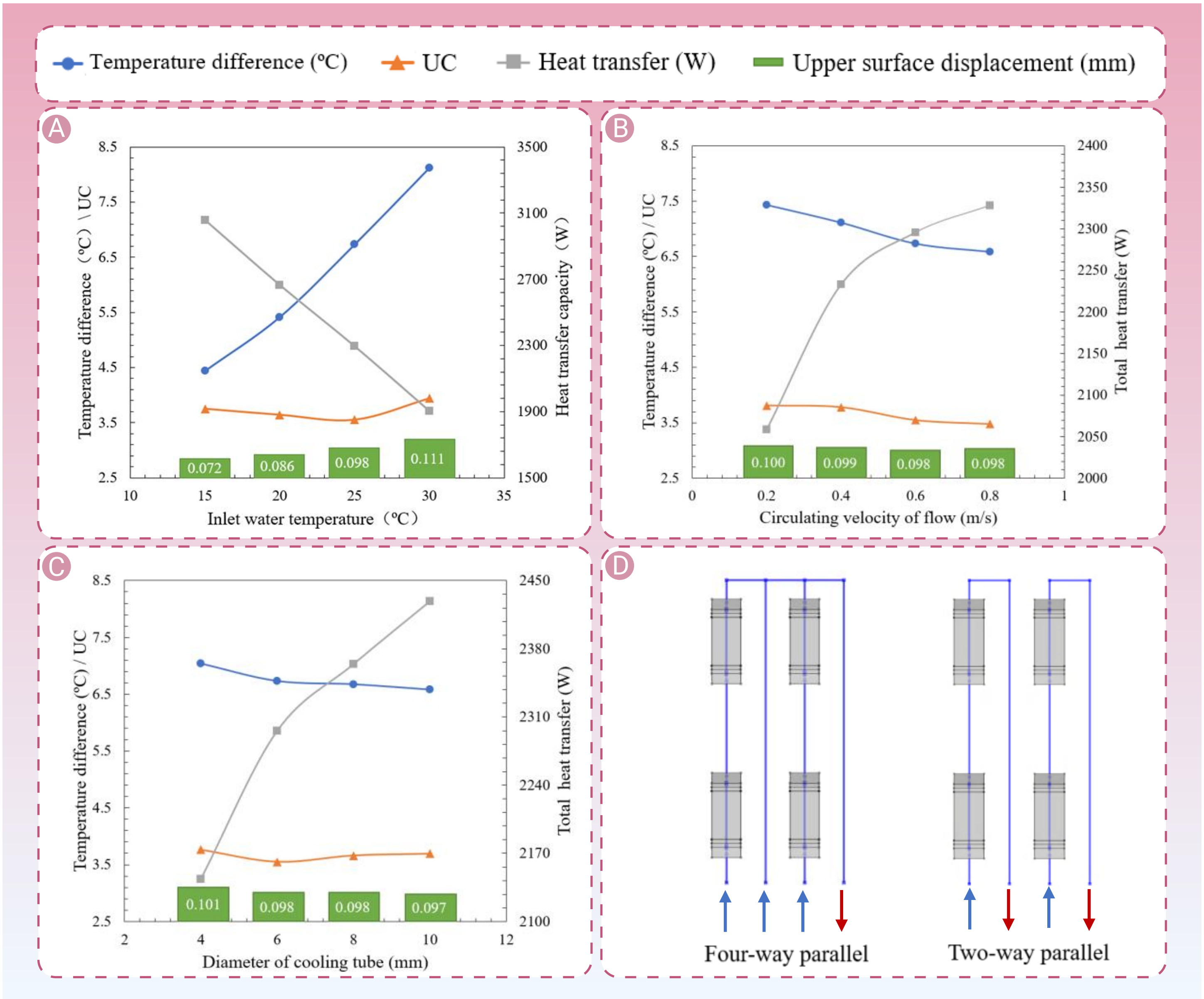


**Figure 8. Influence of operation conditions and tube designs on the thermal management performance** (A) Influence of inlet water temperature; (B) Influence of circulation velocity; (C) Influence of cooling tube diameter; (D) Two connection configurations of cooling tubes

dimensional coupled hydraulic-thermal-mechanical numerical model is established for the ballastless track slab, incorporating various tube designs. This model utilizes the methodology outlined in Materials and Methods Section. The effects of these different tube designs on key performance indicators, such as surface temperature difference, vertical displacement, uniformity coefficient (UC), and total heat transfer of the track slab, are then comprehensively compared and analyzed.

To identify the optimal tube diameter for enhanced thermal performance, a comprehensive analysis of the influence of varying tube diameters was conducted. Figure 8C presents the results pertaining to the surface temperature difference, vertical displacement, uniformity coefficient (UC), and total heat transfer of the corresponding track slab. The study encompassed tube diameters of 4 mm, 6 mm, 8 mm, and 10 mm, while all other boundary conditions remained constant.

With a constant fluid flow velocity, an increase in tube diameter leads to a larger volume flow rate during liquid circulation, effectively enhancing the convective heat transfer coefficient within the tube. As the tube diameters increase, the track slab surface temperature difference and UC decrease, and the corresponding vertical displacement exhibits a linear decline. However, the total heat transfer shows an upward trend. Specifically, for tube diameters of 4 mm, 6 mm, 8 mm, and 10 mm, the surface temperature differences are 7.0 °C, 6.7 °C, 6.7 °C, and 6.6 °C, respectively. The corresponding vertical displacements are 0.101 mm, 0.098 mm, 0.098 mm, and 0.097 mm, respectively. The UC values are 3.76, 3.55, 3.66, and 3.69, and the total heat transfer values are 2144 W, 2296 W, 2364 W, and 2429 W, respectively. Given that the cooling tube should be installed as close as possible to the upper surface of the track slab, the diameter of the cooling tube should not exceed a certain limit. Taking into account the temperature uniformity of the track slab and practical considerations, a cooling tube with an inner diameter of 6 mm is recommended.

To ascertain the optimal tube layout for the track slab module, two distinct tube connections were designed and their respective impacts were comparatively evaluated, as depicted in Figure 8D. In the first configuration, four cooling tubes were interconnected in parallel, wherein two polyline tubes and two straight tubes constituted a cooling unit, with one of the straight tubes serving as the return tube. Conversely, in the second configuration, two cooling tubes were arranged in parallel, comprising a polyline tube and a straight tube that jointly formed a cooling unit, with the straight tube designated as the return tube.

The connection of the cooling tubes significantly influence the efficacy of the thermal management system. Specifically, when comparing the two configurations, the second configuration results in a higher surface temperature difference (6.7 °C vs 7.0 °C) and an increased vertical displacement (0.098 mm vs 0.100 mm) of the track slab. However, it also exhibits a lower uniformity coefficient (UC) value (3.55 vs 3.70) and a reduced total heat transfer (2296 W vs 1960 W). It means the first configuration incorporates fewer return tubes, a higher number of cooling tubes, and maintains a larger heat transfer temperature difference. Therefore, in practical applications, it is advisable to adopt the first four-way parallel cooling tube configuration.

## CONCLUSION

A novel thermal management system, featuring cooling tubes embedded within the ballastless track slab, is introduced to mitigate the risk of thermal damage in hot climates. To facilitate an in-depth analysis, a comprehensive hydraulic-thermal-mechanical coupling model of the track slab is formulated. Additionally, an experimental platform is constructed to verify the accuracy of the numerical model. Subsequent investigations focus on the examination of the temperature field, stress field, and pipeline flow field within the ballastless track slab, both with and without the implementation of the proposed thermal management system, under hot climate conditions. Ultimately, the study delves into optimizing the operational conditions and the design of the cooling tubes to enhance the thermal management efficacy of ballastless track slabs. The principal findings of this research are summarized as follows:

(1) In hot climates, the ballastless track slab exhibits non-uniform temperature and stress distributions, with a maximum temperature difference of 18.3 °C between its upper and lower surfaces (temperature gradient: 0.915 °C/cm, UC value: 5.75). This results in a maximum vertical displacement of 0.156 mm due to temperature stress.

(2) A thermal management system incorporating embedded cooling tubes in the track slab is proposed to enhance temperature uniformity. Compared to a slab without cooling tubes, the proposed system reduces the upper surface temperature and the surface temperature difference to below 7 °C (temperature gradient: 0.335 °C/cm, UC value: 3.55).

(3) The proposed thermal management system also mitigates vertical displacement of the track slab surface, decreasing the maximum displacement by 40% from 0.156 mm to 0.099 mm, thereby preventing thermal damage.

(4) Simulation results indicate that during thermal management, the outlet water temperature of the cooling tubes increases by an average of 0.7 °C, with a maximum heat transfer of 2296 W. Solar power generation is utilized as the power supply, fulfilling both field power needs and cooling requirements through optimal design.

(5) To determine the optimal thermal management configuration, the effects of various operating conditions (inlet water temperature, flow velocity) and cooling tube designs (diameter, layout) were analyzed. The optimal inlet temperature was found to be 25 °C with a flow velocity of 0.6 m/s. A cooling tube with an inner diameter of 6 mm, arranged in a four-way parallel scheme, is recommended.

The research is expected to eliminate the deformation problem caused by the temperature maldistribution of ballastless track slabs and ensure the smooth and effective operation of high-speed railways in hot climates.

### Nomenclature

$C_p$ specific heat, $J/(kg \cdot K)$
$d_h$ hydraulic diameter, $m$
$F_v$ bulk load, $N$
$E$ power generation efficiency
$L$ length of the cooling tube, $m$
$P$ power, $W$
$Q$ heat source, $W$
$T$ temperature, $°C$
$\rho$ density, $kg/m^3$
a absorption rate, 1
$h$ convective heat transfer coefficient, $W/(m^2 \cdot K)$
$k$ thermal conductivity, $W/(m \cdot K)$
p pressure, $N/m^2$
u speed, $m/s$
v velocity vector, $m/s$

### Abbreviations

CA cement emulsified asphalt
COMSOL COMSOL Multiphysics
COP coefficient of performance
GHE ground heat exchanger
GSHP ground source heat pump
PCM phase change materials
PVC photovoltaic cell
PVT photovoltaic-thermal
UC uniformity coefficient

### Subscripts

a atmospheric
c concrete
ch convective heat transfer
ext external
f fluid
grad gradient
h heat
rh radiative heat transfer
ref reference
s solid
sky sky
sr solar radiation
w wind
wall tube wall

## REFERENCES


1. Wu X., Qi L., Zhang T., et al. (2021). A novel kinetic energy harvester using vibration rectification mechanism for self-powered applications in railway. *Energy Convers. Manag.* **228**:113720. DOI:10.1016/j.enconman.2021.113720
2. Deng K., Liu Y., Hai D., et al. (2022). Deep reinforcement learning based energy management strategy of fuel cell hybrid railway vehicles considering fuel cell aging. *Energy Convers. Manag.* **251**:115030. DOI:10.1016/j.enconman.2022.115030
3. Yin F. and Mei S. (2022). The Ministry of Transport releases 2021 Statistical Communique on the Development of the Transport Industry. *Waterway Port* **43**:346. (in Chinese).
4. Pan Y., Zuo L. and Ahmadian M. (2022). A half-wave electromagnetic energy-harvesting tie towards safe and intelligent rail transportation. *Appl. Energy* **313**:118844. DOI:10.1016/j.apenergy.2022.118844
5. Indraratna B., Sajjad M. B., Ngo T., et al. (2019). Improved performance of ballasted tracks at transition zones: A review of experimental and modelling approaches. *Transport. Geotech.* **21**:100260. DOI:10.1016/j.trgeo.2019.100260
6. Zhang T., Wu X., Pan Y., et al. (2022). Vibration energy harvesting system based on track energy-recycling technology for heavy-duty freight railroads. *Appl. Energy* **323**:119673. DOI:10.1016/j.apenergy.2022.119673
7. Yang J., Zhu S. and Zhai W. (2020). A novel dynamics model for railway ballastless track with medium-thick slabs. *Appl. Math. Model.* **78**:907–931. DOI:10.1016/j.apm.2020.06.007
8. Liu X., Zhao P., Dai F., et al. (2011). Advances in design theories of high-speed railway ballastless tracks. *J. Mod. Transport.* **19**:154–162. DOI:10.1007/s40534-011-0021-2
9. Hu J., Bian X., Xu W., et al. (2019). Investigation into the critical speed of ballastless track. *Transport. Geotech.* **18**:142–148. DOI:10.1016/j.trgeo.2019.02.003
10. Köllő S., Puskás A., Köllő G. (2015). Ballasted track versus ballastless track. *Key Eng. Mater.* **660**:219–224. DOI:10.4028/www.scientific.net/KEM.660.219
11. Freudenstein S., Geisler K., Molter T., et al. (2018). Ballastless Tracks. *John Wiley Sons.* DOI:10.1002/9781119380603
12. Huang S., You T., Xie Y. (2025). Radiative cooling for thermal management of ballastless track slab in high-speed railways. *Appl. Energy* **382**:125164. DOI:10.1016/j.apenergy.2025.125164
13. Song L., Liu H., Cui C., et al. (2020). Thermal deformation and interfacial separation of a CRTS II slab ballastless track multilayer structure used in high-speed railways based on meteorological data. *Construct. Build. Mater.* **237**:117528. DOI:10.1016/j.conbuildmat.2020.117528
14. Cai X., Luo B., Zhong Y., et al. (2019). Arching mechanism of the slab joints in CRTSII slab track under high temperature conditions. *Eng. Fail. Analy.* **98**:95–108. DOI:10.1016/j.engfailanal.2019.03.019
15. Zhou R., Zhu X., Ren W., et al. (2022). Thermal evolution of CRTS Ⅱ slab track under various environmental temperatures: Experimental study. *Construct. Build. Mater.* **325**:126699. DOI:10.1016/j.conbuildmat.2022.126699
16. Kosmadakis G., Arpagaus C., Neofytou P., et al. (2020). Techno-economic analysis of high-temperature heat pumps with low-global warming potential refrigerants for upgrading waste heat up to 150 C. *Energy Conver. Manag.* **226**:113488. DOI:10.1016/j.enconman.2020.113488

17. Kev K., Modi N., Milani D., et al. (2023). A comparative life cycle impact assessment for solar heat integration in post-combustion carbon capture. *Energy Conver. Manag.* **297**:117745. DOI:10.1016/j.enconman.2023.117745
18. Ling Z., Lin W., Zhang Z., et al. (2020). Computationally efficient thermal network model and its application in optimization of battery thermal management system with phase change materials and long-term performance assessment. *Appl. Energy* **259**:114120. DOI:10.1016/j.apenergy.2019.114120
19. Mortazavi B., Yang H., et al. (2017). Graphene or h-BN paraffin composite structures for the thermal management of Li-ion batteries: a multiscale investigation. *Appl. Energy* **202**:323–334. DOI:10.1016/j.apenergy.2017.03.051
20. Santamouris M., Pavlou K., Synnefa A., et al. (2007). Recent progress on passive cooling techniques: Advanced technological developments to improve survivability levels in low-income households. *Energy Build.* **39**:859–866. DOI:10.1016/j.enbuild.2007.03.003
21. Jiang H., Zhang J., Zhou F., et al. (2020). Optimization of PCM coating and its influence on the temperature field of CRTSII ballastless track slab. *Construct. Build. Mater.* **236**:117498. DOI:10.1016/j.conbuildmat.2020.117498
22. Zhang J., Jiang H., Ding F., et al. (2020). Effects of metal–ceramic anticorrosion coating on the performance of ballastless tracks at high temperature. *Arch. Civil Mechan. Eng.* **20**:1–14. DOI:10.1016/j.acme.2020.04.016
23. Xiang B., Cao X., Yuan Y., et al. (2018). A novel hybrid energy system combined with solar-road and soil-regenerator: Dynamic model and operational performance. *Energy Conver. Manag.* **156**:376–387. DOI:10.1016/j.enconman.2017.12.044
24. Zhou L., Zhou F., Ge H. (2021). Improving Heat Exchange Performance of Massive Concrete Using Annular Finned Cooling Pipes. *Adv. Mater. Sci. Eng.* **2021**:6715468. DOI:10.1155/2021/6715468
25. Zhang Y., You T., Sun Z., et al. (2022). Performance of thermal management for ballastless track plate of high-speed railway in hot regions. *Case Stud. Therm. Eng.* **40**:102525. DOI:10.1016/j.csite.2022.102525
26. Kreith F. and Manglik R. M. (2016). Principles of Heat Transfer. *Cengage Learn.* DOI:10.1016/B978-0-12-429868-1.00006-2
27. Zhang H. (2019). The Reverse Carnot Cycle Is a Pumping Heat Machine. *Energy* **186**:116–118. DOI:10.1016/j.energy.2019.07.122
28. Feidt M. (2020). Carnot cycle and heat engine: Fundamentals and applications. *Entropy* **22**:348. DOI:10.3390/e22030348
29. Hayat M., Ali D., Monyake K. C., et al. (2019). Solar energy—A look into power generation, challenges, and a solar - powered future. *Int. J. Energy Res.* **43**:1049–1067. DOI:10.1002/er.4505
30. Ling F. and Wu Z. (1999). Numerical simulation of the influence of seepage on temperature field of roadbed in permafrost regions. *J. Glac. Geocry.* **21**:115-119. (in Chinese).
31. Wang X., Chen Y., Xu Y., et al. (2011). Recommended values of soil temperature in Guangzhou based on long-term monitoring. *Guangdong Electric Power* **24**:10–13.
32. Liu W. and Geng Y. (2004). Experimental research on solar absorption coefficient of concrete surface. *Concr. Cem. Prod.* **4**:8-11. (in Chinese).
33. Zhang J. and Liu Z. (2006). Experimental study on convective heat transfer coefficient of concrete in wind tunnel. *J. Civil Eng.* **39**:39–42.
34. Yuan Z., Chen YC. (2012). Engineering Heat Transfer Property-Theoretical Basis and Special Application. Science Press. (in Chinese).
35. Liu S. and Huang Y. (1983). Discussion of sky effective temperature. Journal of Solar Energy 1:65-70. (in Chinese).
36. Department of Building Science of Tsinghua University. (2005). Chinese Architecture-specific Meteorological Data Sets for Thermal Environment Analysis. China Architecture and Building Press. (in Chinese).
37. Kaliakin V. (2018). Introduction to Approximate Solution Techniques, Numerical Modeling, and Finite Element Methods. CRC Press.
38. Liu F., Zeng Z., Wu B., et al. (2016). Study on temperature field of continuous ballastless track for high-speed railway. *J. Rail. Soc.* **12**:87–93.
39. Ou Z. and Li F. (2014). Analysis and prediction of the temperature field based on in-situ measured temperature for CRTS II ballastless track. *Energy Procedia* **61**:1290–1293. DOI:10.1016/j.egypro.2014.11.164
40. Han Z. and Li S. (2011). Temperature measurement and deformation analysis for CRTS II ballastless track slabs. *Rail. Stand. Design* **10**:41–44.
41. Yang R., Li J., Kang W., et al. (2017). Temperature characteristics analysis of the ballastless track under continuous hot weather. *J. Transport. Eng. A Sys.* **143**:04017048. DOI:10.1061/JTEPBS.0000150
42. Bayrak F., Hakan F., et al. (2020). Experimental study for the application of different cooling techniques in photovoltaic (PV) panels. *Energy Conver. Manag.* **212**:112789. DOI:10.1016/j.enconman.2020.112789

## FUNDING AND ACKNOWLEDGMENTS

The authors gratefully acknowledge the funding support from the National Natural Science Foundation of China (No. 52478110) and the Guangdong Basic and Applied Basic Research Foundation (2024A1515010734 and 2020B1515120083).

## AUTHOR CONTRIBUTIONS

All authorsdiscussed the results and approved the final manuscript.

## DECLARATION OF INTERESTS

The authors declare no competing interests.

## DATA AND CODE AVAILABILITY

Data are available from the corresponding author upon reasonable request.